MOLECULAR IMAGING AND BIOLOGY

Mol Imaging Biol (2014) 16:519–528
DOI: 10.1007/s11307-014-0718-3

Published Online: 6 February 2014

World Molecular Imaging Society

RESEARCH ARTICLE

Breast Cancer Cells Imaging By Targeting Methionine Transporters with Gadolinium-Based Nanoprobe

Bita Mehravi,[1] Mehdi Shafiee Ardestani,[2] Maryam Damercheli,[3] Haleh Soltanghoraee,[4] Negar Ghanaldarlaki,[5] Ali M. Alizadeh,[6] Mohammad A. Oghabian,[7] Maryam Shahzad Shirazi,[8] Shabnam Mahernia,[9] Massoud Amanlou[9,*]

[1]*Faculty of Advanced Technologies in Medicine, Iran University of Medical Sciences, Tehran, Iran*
[2]*Department of Radiopharmacy, Faculty of Pharmacy, Tehran University of Medical Sciences, Tehran, Iran*
[3]*Department of Chemistry, Semnan University, Semnan, Iran*
[4]*Reproductive Biotechnology Research Center, Avicenna Research Institute, ACECR, Tehran, Iran*
[5]*Department of Biological Science, School of Science, Science and Research Branch, Islamic Azad University, Tehran, Iran*
[6]*Cancer Research Center, Tehran University of Medical Sciences, Tehran, Iran*
[7]*Research Center for Molecular and Cellular Imaging (RCMCI), Tehran University of Medical Sciences, Tehran, Iran*
[8]*School of Chemistry, University College of Science, University of Tehran, Tehran, Iran*
[9]*Department of Medicinal Chemistry, Faculty of Pharmacy and Drug Design and Development Research Center, Tehran University of Medical Sciences, Tehran, Iran*

Abstract

Purpose: Early cancer diagnosis using MRI imaging is of high global interest as a non-invasive and powerful modality. In this study, methionine was conjugated on gadolinium-based mesoporous silica nanospheres to evaluate intra-cellular uptake and its accumulation in human breast cancer cells.

Procedures: The contrast agent was synthesized and characterized using different techniques including N_2 physisorption, thermal gravimetric analysis, dynamic light scattering, and inductively coupled plasma atomic emission spectroscopy (ICP-AES). The intra-cellular uptake of Gd^{3+} was measured by ICP-AES, fluorescent microscopy, and flow cytometry. Finally, cellular and tumor MR imaging were performed to determine *in vitro* and *in vivo* relaxometry.

Results: According to the results, the contrast agents accumulated in tumor cells both *in vitro* and *in vivo*. There was no significant cellular toxicity on either normal or cancer cells along with strong intense signal on T_1 compared to the unlabeled cells.

Conclusions: The results showed that the novel contrast agent could become a useful tool in early detection of cancer.

Key words: Cell imaging, Gadolinium, Mesoporous silica nanospheres, Methionine, MRI

Introduction

Contrast agents (CAs) containing paramagnetic agents, used in magnetic resonance imaging (MRI), are non invasive and powerful diagnostic tools in cancer early

Electronic supplementary material The online version of this article (doi:10.1007/s11307-014-0718-3) contains supplementary material, which is available to authorized users.

Correspondence to: Massoud Amanlou; *e-mail:* amanlou@tums.ac.ir

diagnosis and biomedical research due to their ability to provide high-resolution anatomical images of soft and in-depth anatomical tissues. Metal ions (predominantly gadolinium ions, Gd^{3+}) are widely used to improve the diagnostic confidence in MRI [1]. These CAs exhibit time-dependent magnetic dipolar interaction with the surrounding water protons and improve the MRI sensitivity by decreasing the proton relaxation time T_1 [2, 3]. However, currently used CAs are mainly small gadolinium chelate molecules with a lack of sensitivity and often do not provide suitable contrast enhancement in early cancer stages [1]. Despite progress in design and preparation of CAs, many of them are still limited by low specificity, selectivity, and toxicity [1]. To overcome these limitations, it is necessary to accumulate a large number of CAs at the target site by recognizing specific molecules that are over expressed in the given pathological area [3]. Recent advances in nanotechnology have improved the properties of CAs for these biomedical applications [4]. Among nanoparticles, porous materials are ideal platforms for a large number of CAs imaging due to their high-surface area and porosity. Mesoporous silica nanospheres (MSN) have high-surface area and high-pore volume. They also have internal surface (i.e., cylindrical pores) and external surface (i.e., exterior particle surface) [5]. MSNs are comprised of a honeycomb-like porous structure with hundreds of empty channels that are able to encapsulate relatively large amounts of CAs. These characteristics allow selective functionalization of the internal and/or external surfaces of MSNs with different moieties. In addition, attaching a target group such as antibodies, peptides, aptamers, carbohydrate, e.g., glucose [6] and folic acid [7] on the surface of MSN can be used to increase the specific accumulation of these nanoparticles within the desired cancerous tissue or on its surface. Amino acids are one of these target groups [8, 9]. Additionally, a significant glutamine uptake by the cancerous cells has been reported [3, 9–11]. Tumor cells have an increased demand for amino acids compared to normal cells [3, 8–11]. In fact, proliferating cells consume more methionine (and its derivatives) than their normal cells [12, 13].

Amino acid uptake is increased in tumor, which is often exploited for tumor detection and staging and to assess therapeutic treatment, using radiolabeled amino acids such as methionine [12] by single-photon emission computed tomography or positron emission tomography techniques [10–13]. Methionine is an essential amino acid which is necessary for growth and development; since proliferating cancer cells absorb more methionine, it is transported into cancer cells faster than normal cells [11]. Many studies have reported using liposomes and nanoparticles labeled with Gd^{3+} complexes targeted to amino acid transporters in order to image the tumor angiogenesis [14–16].

In this study, we introduce a novel Gd^{3+}-based contrast agent for cancer cell imaging. Our study focuses on the exploitation of the methionine transport system in order to incorporate Gd^{3+}-based mesoporous silica nanospheres conjugated with methionine (Met-MSNs-Gd^{3+}) into the cancer cells. Therefore, we report here the synthesis, physicochemical analysis, application of Met-MSNs-Gd^{3+}, as well as *in vitro* and *in vivo* studies, along with cellular uptake behavior and its application in MRI cell imaging.

Materials and Methods

Chemical

Fetal bovine serum (FBS), penicillin sterptomycin and $GdCl_3.6H_2O$ (99 %) and Chelex 100 (Na^+ form) were purchased from Sigma Aldrich Co. (USA), aminopropyltriethoxysilane (APTES, 99 %), tetraethyl orthosilicate (TEOS, 98 %), anhydrous ethanol (EtOH, 99.5 %), cetyltrimethylammonium bromide (CTAB, 98%), 3-(trimethoxysilylpropyl) diethylenetriamine (99.9 %), sodium hydroxide, anhydrous N, N-dimethyl formamide (DMF, 99.8 %), and toluene (99.8 %) provided from Acros Co. (Belgium) and used without further purification. Dialysis bag with 500–1,000 Da cut off obtained from the Spectrum Lab. (USA). Magnevist® obtained from Bayer HealthCare Pharmaceuticals Inc., (Montville, NJ, USA). Other materials were purchased from Merck KGaA (Darmstadt, Germany).

Human breast cancer cell lines (MCF-7), human kidney cell line (HEK 293) and murine mammary adenocarcinoma cells (derived from M05 cell line) were provided from National Cell Bank of Pasteur Institute of Iran.

Animals

All the animal studies have been conducted according to relevant national and international guidelines of Tehran University of Medical Sciences. All inbred female BALB/c mice (6–8 weeks old, purchased from Iran Pasteur Institute) were maintained in large group houses under 12-h dark and light cycles, and were given access to food and water *ad libitum*.

Synthesis of Gd^{3+}-Based Mesoporous Silica Nanoparticles

The MSN were synthesized according to the Stober method [2, 17]. Briefly, CTAB (1.0 g) was dissolved in distilled water (480.0 ml) which contained NaOH (4.0 ml, 2 M) and the solution was heated at 80 °C. TEOS (5.0 ml) was added drop wise over 15 min to the mixture. After stirring for 3 h at 80 °C, MSN were isolated by filtration and washed twice with distilled water and ethanol.

Silanization of Mesoporous Silica Nanoparticles (MSN-NH_2)

MSN (1.0 g) were dispersed in anhydrous ethanol (100 ml) and sonicated for 10 min. APTES (1.0 ml) was added to the solution in approximately 15 min and the reaction was stirred for 12 h. The resulting solution was centrifuged at 5,000 rpm for 25 min and residues were redispersion in water to remove unreacted APTES [17].

Surfactant Extraction

CTAB template was extracted from MSN-NH_2 (1.0 g) by HCl (5.0 ml) in ethanol (120.0 ml) under reflux. After 12 h, the reaction mixture was centrifuged at 6,000 rpm for 25 min at RT. The extracted MSN-NH_2 was washed three times with ethanol and was stored as dispersion in ethanol (96 %) for further usage [17].

Si-DTPA Complex Synthesis

The diethylenetriamine pentaacetic acid dianhydride (DTPA-DA) synthesis procedure has been described previously [18]. DTPA-DA (3.57 mg) was dissolved in anhydrous DMF (10.0 ml) under a steady flow of N_2, and then N, N-dicyclohexylcarbodiimide (DCC) (4.5 mg), 1-hydroxy-benzotriazole (1.6 mg), triethylamine (2.0 ml), and activated molecular sieve 3 Å (100 mg) were added to the medium. The reaction mixture was stirred at RT for at least 30 min, the reaction temperature increased to 100 °C, and then APTES (1.0 mg) was added. The reaction mixture was heated at 100 °C for 24 h and finally, it was centrifuged (6,000 rpm, 25 min) and redispersed in water to remove unreacted APTES. After washing with water and ethanol, a white powder was obtained in high yield (>90 %). DTPA-DA: Fourier transform infrared spectroscopy (FT-IR) (KBr, per centimeter): 906; 1,203; 1,089; 1,638; 2,927; and 3,380. MS: *m*/*z* %: 596.2. DTPA-APS: FT-IR (KBr, per centimeter): 1,638.53; 1,730.95; 1,818.49; 2,555.90; 2,714.65; and 3,103.84. MS (ESI negative ion): *m*/*z* 357.3 [M-H] for the silanetriol from a basic solution. The schematic synthesis of DTPA-DA is shown in Fig. S1.

Preparation of Si-DTPA-Gd^{3+} Complex

Si-DTPA (100.0 mg) dissolved in distilled water (4.0 ml) was stirred at RT. A solution of $GdCl_3$ (300.0 µl of a 0.5 M) was added drop wise into the solution. The solution pH was adjusted to about nine with addition of NaOH (1 M) [19]. After stirring for 3 h at RT, the reaction mixture was dialyzed by using a dialysis bag (cut off point 500–1,000 Da) against phosphate buffer solution (PBS) to ensure the removal of unreacted Gd^{3+}.

Synthesis

The schematic synthesis procedure of mono (3-aminopropyl triethoxysilyl)diethylenetriamine pentaacetic acid (Si-DTPA) is shown in Fig. S1. The Si-DTPA-Gd^{3+} complex were identified by using ultraviolet spectroscopy (see Fig. S2).

Loading Si-DTPA-Gd^{3+} in MSN-NH_2

The MSN-NH_2 (200.0 mg) was refluxed with a Si-DTPA-Gd^{3+} complex (0.5 ml, 0.1 M) in anhydrous EtOH. The resulting Gd^{3+}-based MSN-NH_2 (NH_2-MSN-Gd^{3+}) was centrifuged at 8,000 rpm for 15 min then washed with water and ethanol subsequently [2].

Carboxylic Acid-Functionalized MSN (COOH-MSN-Gd^{3+})

A dispersion of NH_2-MSN-Gd^{3+} (553.0 mg) in anhydrous DMF (20.0 ml) was added to succinic anhydride (200.0 mg in anhydrous DMF). The mixture was stirred under N_2 over night. The COOH-MSN-Gd^{3+} was isolated by using centrifuge (6,000 rpm, 10 min), and washed three times with DMF [20].

Synthesis of Met-MSN-Gd^{3+}

A dispersion of COOH-MSN-Gd^{3+} (10.0 mg) in anhydrous DMF was sonicated for 10 min. The coupling agent [DCC (0.2 mg)/HOBT (0.1 mg)] was added to the solution and the reaction mixture was stirred at RT for at least 30 min. Benzyl-carboxyl protected-methionine (30.0 mg) was added and the reaction mixture was stirred at RT for 72 h under N_2. The reaction mixture rinsed with DMF and water. The amino acid derivative was dissolved in 1:1 methanol/tert-Butyl alcohol. The Pearlman's catalyst [$Pd(OH)_2$-C] was added under a hydrogen atmosphere and was allowed to stir until completed. Unbounded methionine was removed by dialyzing against PBS to ensure the removal of all free methionine. The schematic synthesis of Met-MSN-Gd^{3+} is shown in Fig. S3.

Preparation of Fluorescent-Doped MSN (MSN-FITC)

Rhodamine B isothiocyanate (5.0 mg) was dissolved in anhydrous ethanol (20.0 ml) and 3-aminopropyltriethoxy silane (4.0 µl) was added to the solution [21]. The reaction mixture was stirred at RT in darkness for 24 h. MSN–NH_2 (50 mg) was suspended in dried toluene (5.0 ml) and then a solution of rhodamine-APS (100.0 µl, 6 mM) was added. The mixture was refluxed overnight. MSN-NH_2-FITC was isolated by centrifuging, and washed with water and ethanol twice. A dispersion of MSN-NH_2-FITC (500.0 mg) in anhydrous DMF (20.0 ml) was added to succinic anhydride (200 mg in anhydrous DMF). The mixture was stirred under N_2 over night. The MSN-COOH-FITC was isolated by centrifuge (6,000 rpm, 10 min), and washed twice with anhydrous DMF. A dispersion of MSN-COOH-FITC (5.0 mg) in anhydrous DMF (20.0 mM) was sonicated for 15 min. The coupling agent [DCC (1 mg)/HOBT (0.5 mg)] was added to the solution and the reaction mixture was stirred at RT for 30 min in the dark. Benzyl-carboxyl protected-methionine (15.0 mg) was added and the reaction mixture was stirred at RT for 24 h under N_2. After removing the benzyl group, the reaction mixture was rinsed with DMF and then the Met-MSN-FITC powder was obtained.

Cell Culture

Human breast cancer (MCF-7) and kidney (HEK 293) cell lines cultured at 37 °C and 5 % CO_2 by using standard cell culture media, containing Dulbecco's Modified Eagle Medium (DMEM). The cell culture medium was supplemented with 10 % FBS and 1 % penicillin–streptomycin.

Cell Viability Test

For the MTT assay, the MCF-7 cell line (5×10^5 cells per well) was incubated with various amounts of Met-MSN-Gd^{3+} (100, 50, 10 μg/ml), MSN-Gd^{3+} (100 μg/ml) and Magnevist (100 μg/ml) in a 96-well microplate for 24 h with untreated cells as control. Each concentration was tested in triplicate. The cells were washed with PBS before adding MTT solution (20 μl of 5 mg/ml MTT solution) to each well. After 4 h, absorbance of purple formazone was measured by using BioTek's absorbance microplate readers at 450 nm (Fig. 1).

Intra-cellular Uptake of Met-MSN-Gd^{3+}

To detect intra-cellular uptake of Met-MSN-Gd^{3+} and MSN-Gd^{3+}, MCF-7 and HEK 293 cell lines were re-plated into 6-well plates at a concentration of 1×10^5 cells per well and incubated at 37ºC and 5 % CO_2 for 24 h. Met-MSN-FITC (fluorescein isothiocyanate, 100 μM) was added to each well (1-ml media). Cells were incubated at 37ºC and 5 % CO_2 for 2 h, washed twice with PBS (500 μL), and then centrifuged at 1,000 rpm for 4 min and reconstituted in 100 μL of PBS. The intra-cellular fluorescent activity was counted and analyzed. The resulting labeled cells were imaged using a fluorescent microscope and analysis of quantitative cell uptake was performed by flow cytometer [19]. Finally, the intra-cellular uptake of Gd^{3+} ions was determined by inductively coupled plasma atomic emission spectroscopy (ICP-AES), quantitatively. The measurements were performed in triplicate and the mean ± SD of the results were calculated.

MR Measurement

The relaxation times of Met-MSN-Gd^{3+} were measured at different concentrations by using different spin echo and gradient echo protocols in 3T MRI with a head coil. For T_2 measurement, multiple spin echo protocols were used. In total, 32 echoes with an echo spacing of 2 ms were obtained. The first echo time (T_E) was 13.2, TR was 3,000 ms, matrix=256×256; slice thickness=1.5 mm, and non-averaged. A FLASH protocol was used to calculate T_1 maps. Repetition times of T_R=20, 50, 100, 200, 400, 600, 1,000, 2,000 and 3,000 ms; T_E was 12 ms; matrix=256×256; slice thickness=1.5 mm, and non-averaged.

In Vitro MRI Preparation

The MCF-7 cell line (1×10^5) was incubated with different doses of Met-MSN-Gd^{3+} (0.8, 0.4, and 0.2 mM) for 1 h. The labeled cells were washed with PBS, trypsinized, and centrifuged at 1,000 rpm for 5 min at 37 °C. Subsequently, cells were re-suspended in an equal volume of DMEM culture media and 2 % agarose gel at 37 °C, and were immediately transferred into the phantom tubes for MR procedure. The relaxation rates were measured using 3 T MRI scanners. The untreated cells were used as the control group. For quantitative analysis, the MRI images were analyzed by DICOM software version 1.3.0.5. (MEDAV GmbH Company).

In Vivo MRI Preparation

The murine mammary adenocarcinoma cells were trypsinized and re-suspended in 10-fold excess culture medium. After centrifugation, cells were re-suspended in serum-free medium, and 1×10^6 cells injected subcutaneously in a final volume of 0.1 ml using a 21-gauge needle in the left flank of BALB/c mice under ketamine and xylazine (10 mg/kg, i.p) anesthesia. Tumor growth was visible 2–3 weeks post injection. The tumor images were obtained 15 min after tail vein injection of 5.0 μM/kg/BW of Met-MSN-Gd^{3+}, using MRI scanner.

Results

Synthesis of Met-MSN-Gd^{3+}

APTES was used to introduce amine groups on the surface of MSN by silanization. The carboxylic acid group was

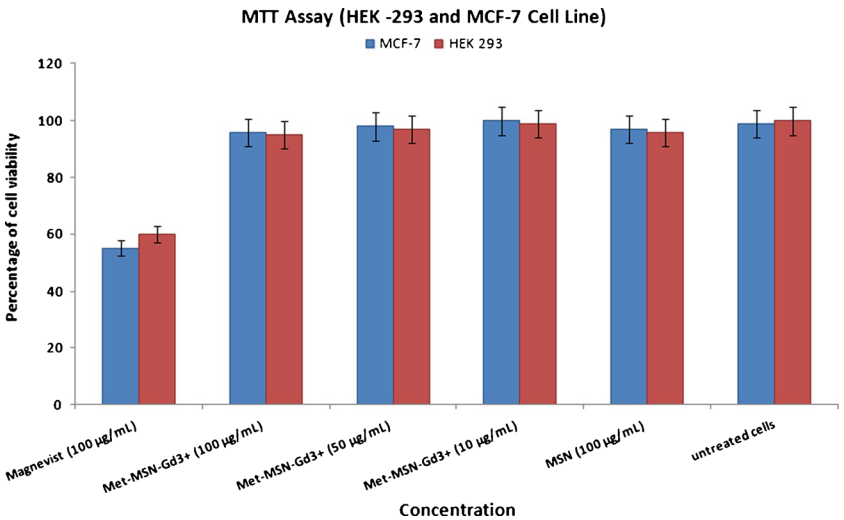

Fig. 1 MTT results of 48 h of Met-MSN-Gd^{3+}, MSN-Gd^{3+}, and Magnevist exposure to human breast cancer cell lines (MCF-7), and human kidney cell lines (HEK-293), no significant toxic effect was observed ($P<0.05$).

produced by a ring opening linker elongation reaction of the amine group with succinic anhydride. These conversions were qualitatively tested by salicylaldehyde. Upon addition of salicylaldehyde, the MSN–NH_2 (without surfactant) was turned yellow immediately, indicating the presence of amino groups, whereas observation showed that extracted MSN–COOH was hardly yellow even after 24 h. This indicated that most of the amino groups were converted to COOH as reported by others previously [20].

Nitrogen gas adsorption measurements indicated that the surfactant-extracted MSN is highly porous with a surface area of 1,189 m^2/g and an average pore diameter of 2.5 nm and total pore volume of 0.59 cm^3/g. On the other hand, Met-MSN-Gd^{3+} reduced surface area of 22.5 m^2/g, a pore diameter of 1.0–1.5 nm and total pore volume of 0.086 cm^3/g (see Table S1).

TGA analysis of extracted MSN showed a weight loss of 1.0 % in the 160–290 °C temperature range. This result indicates that the surfactant removed during extraction (see Fig. S4).

The modification of mesoporous silica surface accompanied by a change in silica surface nanoparticle charge, which was confirmed by zeta potential measurements (see Table S2). The MSN–NH_2 nanoparticle aggregated in water at pH value 7. In this study, the solution showed alkalescence and a low negative zeta potential about +3.7 mV, so MSN–NH_2 aggregated in a short time [20–23]. Pore size distribution of surfactant-extracted MSN and MSN-Gd^{3+}-Met are shown in Fig. S5.

Fourier transform infrared spectroscopy was used to confirm the existence of functionalized MSNs in the region of 400–4,000 cm^{-1}. The infrared spectrum of MSN showed a broad absorption band at 3,200–3,600 cm^{-1} corresponding to the silanol-OH bond and

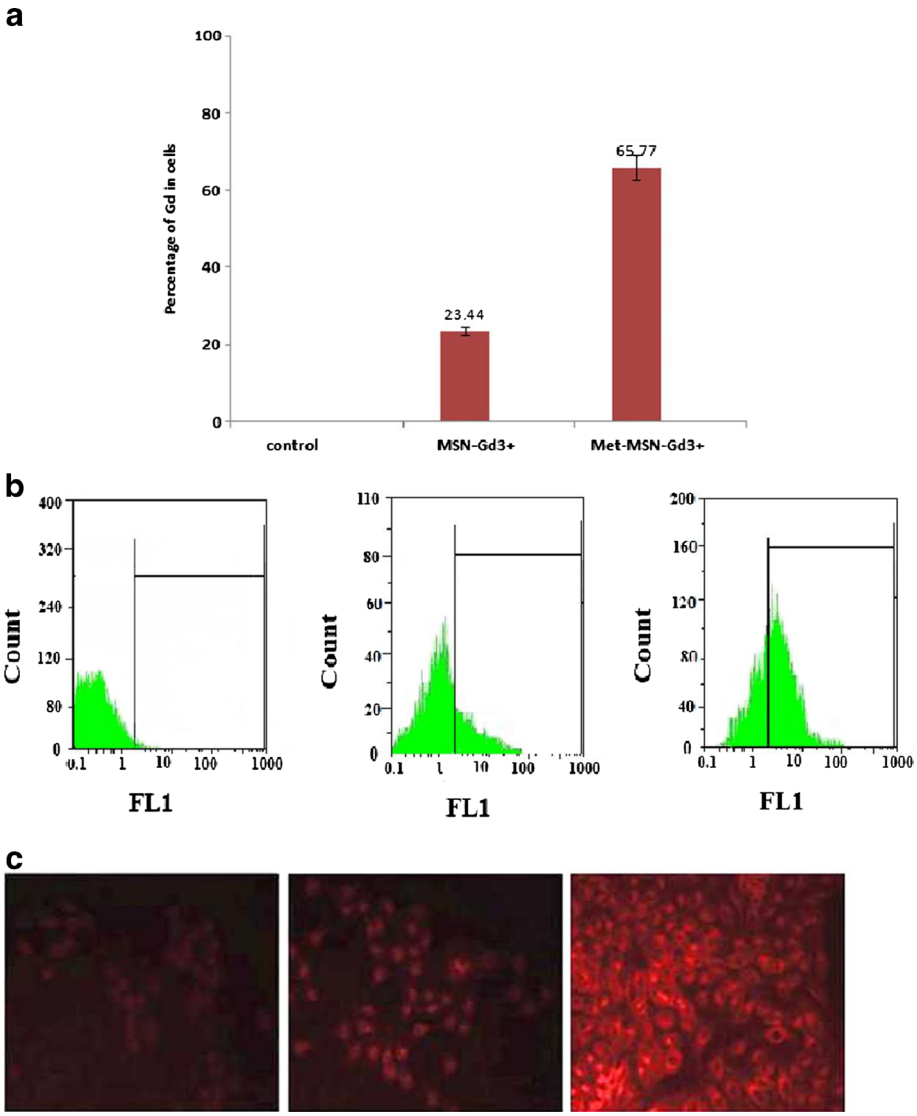

Fig. 2 Intra-cellular uptake of MSN-Gd^{3+} and Met-MSN-Gd^{3+} by different techniques: ICP-AES (**a**), flow cytometry (**b**), and fluorescent Microscopy (**c**). Notes: The insets show the purity of the cell populations, 1 × 10^5 MCF-7 cells in mL media; Met-MSN-Gd^{3+} -labeling cell after 2 h. Results indicated the Methionine effect on intra-cellular uptake.

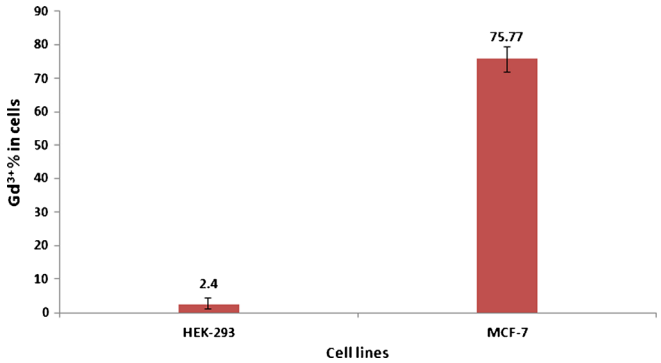

Fig. 3 The difference of intra-cellular uptake of Met-MSN-Gd^{3+} in human breast cancer cell lines (MCF-7) and normal kidney cells (HEK-293).

strong absorption of the siloxane (Si−O−Si) group at 1,094 cm^{-1}. When methionine was grafted onto the MSNs, the spectrum showed a new broad absorption band at 3,100–3,600 cm^{-1} corresponding to the carboxylic acid (-COOH) bond and an absorption of the siloxane (Si−O−Si) group at 1,062 cm^{-1}. An amide carbonyl (−NH−C=O) stretch mode at about 1,655 and 1,501 cm^{-1}. These results indicate that methionine was incorporated into MSNs (see Fig. S6).

Scanning and transmission electron microscopy was used to evaluate MSN morphology and size. The images show that there was no change in MSN morphology after conjugation of methionine onto the surfaces of the MSNs, extraction of the surfactant, or upon grafting of the Gd3+-DTPA-chelated molecule (see Fig. S7 and S8).

The high-angle XRD patterns of MSN and Met-MSN-Gd^{3+} are shown in Fig. S9. The MSN exhibits a single strong peak in the XRD pattern followed by two additional peaks which are assigned to the (100), (110), and (200) reflections of a hexagonal lattice. The Met-MSN-Gd^{3+} sample displays the same reflections with a small peak shift to the high angles.

The Cell Viability Test

Figure 1 shows a comparison of MCF-7 cell line incubated for 24 h at different concentrations (10, 50, and 100 μg ml^{-1}) of Met-MSN–Gd^{3+}, MSN–Gd^{3+} (100 μg ml^{-1}), and Magnevist (100 μg ml^{-1}). The values for all Met-MSN-Gd^{3+} concentrations were similar to control (untreated cells), indicating that cell viability was not affected at the concentration range, whereas Magnevist showed significant toxicity effects ($P<0.05$).

Intra-Cellular Uptake of Met-MSN-Gd^{3+} Into Tumor Cells

Figure 2 shows the affinity of tumor cells to the Met-MSN-Gd^{3+} in comparison with the nonspecific precursor MSN-Gd^{3+}. Fluorescence microscopy as well as flow cytometry studies on tumor cells showed 23 %±0.09 intra-cellular uptake for nanospheres but a high intra-cellular uptake ratio of 65.77 %±1.7 was obtained for Met-MSN-Gd^{3+}. Data confirms the important role of conjugate methionine in nanostructure of Met-MSN-

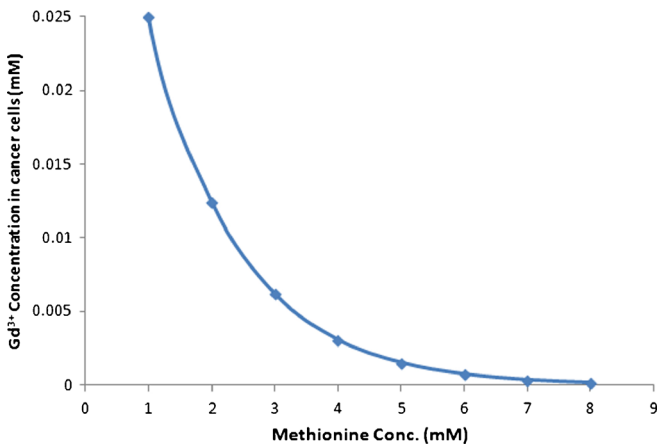

Fig. 4 Effect of the addition of methionine to the incubation medium on the amounts of internalized Met-MSN-Gd^{3+} into MCF-7 cell lines.

Gd^{3+}; these results were also confirmed by ICP-AES data.

To assess the *in vitro* capability of the Met-MSN-Gd^{3+} to discriminate between tumor and normal cells (see cell culture in Materials and Methods), an ICP-AES analysis was carried out on MCF-7 and HEK-293 cell lines. Figure 3 shows that Met-MSN-Gd^{3+} intra-cellular uptake in human breast cancer cell (MCF-7) was higher than that found in human normal kidney cells (HEK-293). Figure S10 also shows that cells labeled with Met-MSN-Gd^{3+} shows a more intense signal on the T_1-weighted spin echo image than the unlabeled cells. This indicated efficient uptake of the Met-MSN-Gd^{3+} for cancer cell imaging.

To demonstrate the methionine graft on the surface of the MSN-Gd^{3+} (as the vehicle for the internalization through the amino acid transporting system), competition evaluations with free methionine were carried out. Figure 4 shows that the intracellular uptake of the Met-MSN-Gd^{3+} by MCF-7 cell decreases as the concentration of the free methionine added to the culture medium increases.

In Vitro MRI Experiments

To find the enough amount of internalized Met-MSN-Gd^{3+} for MRI visualization of cancer cells, an *in vitro* MRI experiment

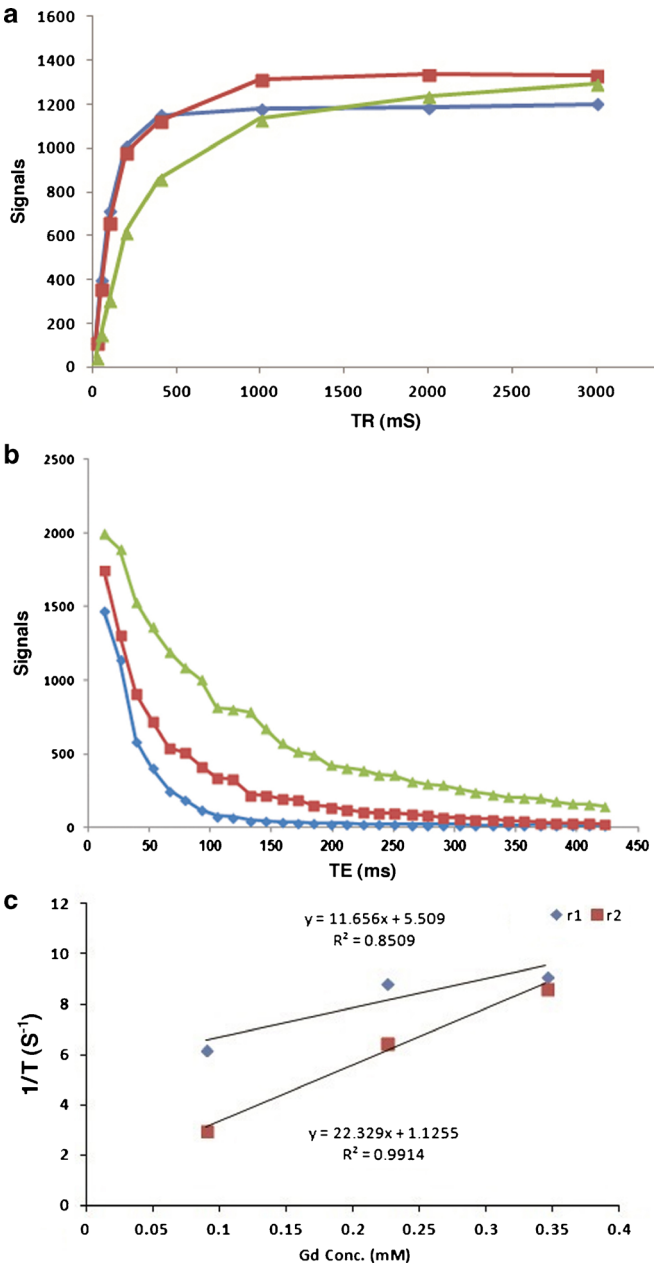

Fig. 5 T_2 data based on spin echo and gradient echo protocols (**a**). T_1 data based on spin echo and gradient echo protocols (**b**). The r_1 and r_2 relaxivity curves of Met-MSN-Gd^{3+} in cancer cells by 3T scanner (**c**).

was performed. For this purpose MCF-7 cells were incubated for 1 h in the presence of 100 μM of Met-MSN-Gd^{3+}. Results show that labeled cells with Met-MSN-Gd^{3+} displayed a strong and intense signal on the T_1-weighted spin-echo image with respect to the untreated cells which demonstrates an efficient uptake of the Met-MSN-Gd^{3+}. The r_1 and r_2 values were measured after cell uptake by MRI, and found 11.65 and 22.33 mM^{-1} s^{-1} in cells, respectively. Relaxometric investigations shows more insights into the intra-cellular localization of Met-MSN-Gd^{3+}. Figure 5 demonstrates the observed relaxation rates (R_1) vs. the number of Gd^{3+} ions per cell. On the basis of these results, the Met-MSN-Gd^{3+} is considered for the following *in vitro* and *in vivo* studies.

Cancer Cell Imaging

For cell imaging, about 4×10^3 labeled cells and 4×10^3 unlabeled cells was injected in the right and left dorsal flank of mice, respectively. Figure S11 showed that the labeled cells had very good signals after 10 min when compared to the unlabeled cells.

In Vivo Targeting of Methionine Receptors

To evaluate the *in vivo* capability of the Met-MSN-Gd^{3+} and discriminate between tumor and normal tissues, a MRI study was carried out on animal models. Results indicated that the tumor images was obtained a few minutes after the injection and the amount of internalized Met-MSN-Gd^{3+} is large enough to yield a significant effect on the MRI signal intensity (Fig. 6).

Statistical Analysis

Multi group comparisons were carried out by one-way ANOVA. Statistical significance for cell toxicity was set at $P<0.05$. Results are expressed as mean ± SD.

Discussion

In the present study, we used MSN as a nanocarrier for cancer imaging. The development of novel CAs that accumulates at the target tissues is critical for cancer cell imaging especially in MRI. Conjugation of methionine on the surface of MSN can be used to increase the specific accumulation of these nano carriers within the desired cancerous tissue. Recent studies demonstrate that conjugating functional groups on the surface of MSN, can affect the cell uptake of MSN. Most notably, D-glucose was conjugated to MSN and DTPA labeled with Gd^{3+}, was investigated *in vitro* and *in vivo* for human breast cancer cell imaging [18, 24, 25]. In addition, a nano-dendrimer was synthesized and conjugated with C595 MAb against human breast cancer cells, followed by chelating agent with Gd^{3+} and used as a dual-nanosized probe for detection and treatment [26]. Other researchers have developed a reporter Gd^{3+}-DOTAMA-C_6-Gln, where the glutamine residue was covalently bound to the Gd^{3+} chelate through a C6 spacer as a contrast agent for MRI [3].

It is cited that internalization of MSN is due to their strong affinity for clathrin-coated vesicles because of their siliceous composition; clathrin pits have been identified as the main mechanism of cell entry of non-cell membrane integrity [25]. After grafting methionine on the MSN surface, internalization occurs through a receptor-mediated endocytosis. As a result they are internalized in to MCF-7 cells by specific cellular uptake and transported into the cytoplasm based on up-regulation of methionine transport system.

The surface charge property, zeta potential, of Met-MSN-Gd^{3+} was −27.4 which showed that Met-MSN-Gd^{3+} with high-surface charges can easily escape endosomal entrapment. This phenomenon could be attributed to the osmotic pressure produced by high density of ions surrounding the surface of highly charged MSN [5]. To allow the interaction Met-MSN-Gd^{3+} with the transporter on the cell membrane, it is necessary to introduce an aliphatic spacer between the

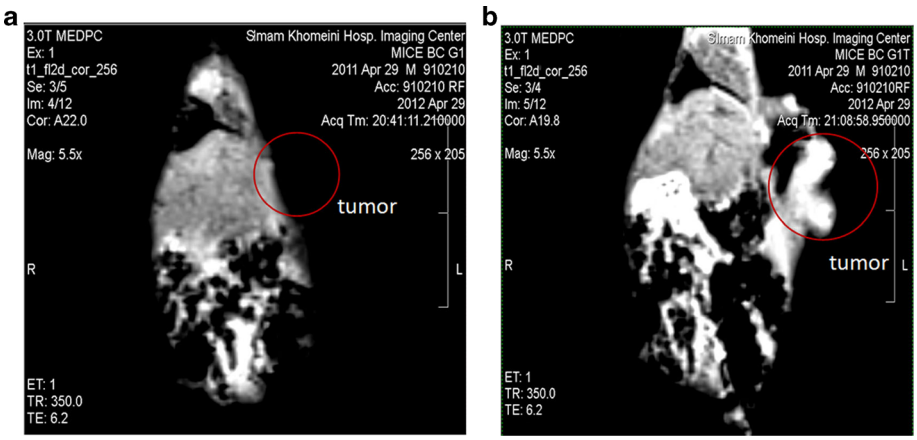

Fig. 6 Breast cancer tumor imaging using MRI: pre-contrast (**a**) and 15-min post-contrast (5 μmol/kg) (**b**). This result shows the ability of Met-MSN-Gd^{3+} in enhancing the T_1-weighted liver images at lower doses.

MSN and methionine moiety. In this procedure, the succinic anhydride probably can cover the curved surface completely. After reacting methionine with COOH, methionine can cover the curved area. The accessibility of the methionine on the surface is expected to be great for the curved surface and exhibit great freedom of movement [25].

Other studies have also aimed at increasing CAs or nanoparticles uptake by cancer cells by conjugating them with methionine [11–13]. In one study, researchers conjugated methionine to DTPA and an anionic linear globular dendrimer G2, which was labeled with ^{99m}Tc, and examined cancer cell imaging *in vitro* and *in vivo* and also studied cellular uptake of these components in the human colon adenocarcinoma (HT 29) cell line. The results indicated that the cellular uptake of ^{99m}Tc-DTPA-Met after 2 and 4 h were about 22 and 43 %, respectively [11]. Our results indicated that cellular uptake of Met-MSN-Gd^{3+} after 2 h was about 65.77 %±1.7. The cellular uptake was higher than ^{99m}Tc-DTPA-Met and ^{99m}Tc-Dendrimer–Met. This difference is probably related to nanoparticles properties (size, charge) and cancer cell lines. Furthermore, increasing amounts of free methionine in the culture medium clearly inhibits the cellular uptake. These results helped to demonstrate that methionine is the vehicle for the interaction of this contrast agent with cancer cells.

The *in vitro* studies on human breast cancer cells such as MCF-7 showed that Met-MSN-Gd^{3+} was taken up by cells 2–7 times more efficiently than the MSN-Gd^{3+}which shows the importance of methionine group in internalization of Met-MSN-Gd^{3+}. Another interesting point is the differential intracellular uptake of methionine into cancerous and normal cells: the amount of Met-MSN-Gd^{3+} in human breast cancer cells was higher than that in normal kidney cells. This result supports the methionine transporter up-regulation in cancer cells and that internalization of Met-MSN-Gd^{3+} occurs through a receptor-mediated endocytosis [27].

Biocompatibility is a major concern when Met-MSN-Gd^{3+} is introduced into cells. Results showed no significant changes in cells viability treated with Met-MSN-Gd^{3+} compared to control group (Fig. 1), while Magnevist showed significant cell toxicity. The results are consistent with our previous studies that show Met-MSN is excellent contrast agent delivery carrier [28].

Furthermore, since Met-MSN-Gd^{3+} is designed as a contrast agent, relaxivities are essential parameters. The r_1 and r_2 values after intra-cellular uptake by MRI were found 11.65 and 22.33 mM^{-1} s^{-1} in cells, respectively, and the r_2/r_1 ratio was 1.9. This result showed that Met-MSN-Gd^{3+} is a good T_1-weighted contrast agent. We attributed the enhanced MR relaxivity to the accessibility of cellular water molecules at Gd^{3+}. Relaxometric investigations showed that it is possible to get more insights into the intra-cellular localization of Met-MSN-Gd^{3+}. This is due to the endosomal compartmentalization of water molecules that are an additional barrier for the Gd^{3+} to access water. Comparing the relaxivities of Met-MSN-Gd^{3+} and Magnevist (r_1 value of 4.1 mM^{-1} s^{-1} under the same condition) [2] show that the Met-MSN-Gd^{3+} can be a better contrast agent than Magnevist. A significant positive signal enhancement in the T_1-weighted image was observed for the labeled cells when compared to the unlabeled cells (Fig. S11). The T_1-weighted image enhancements were related to the reduction of T_1 relaxation times.

Moreover, in the present study, a tumor-oriented MR-contrast agent based on Met-MSN-Gd^{3+} targeted to the methionine receptors that are over expressed in tumor cells has shown the ability of Met-MSN-Gd^{3+} in enhancing the T_1-weighted images. Other researcher also synthesized MSNs, labeled with Gd^{3+}-DTTA, as T_1-contrast agent without targeting group [2] and demonstrated the efficacy of MSN-Gd^{3+} as T_1-contrast agents both *in vitro* and *in vivo*. Our results confirm the results that MSN-Gd^{3+} has good potential in early cancer diagnosis [2]. The effectiveness of Met-MSN-Gd^{3+} as an *in vivo* MR-contrast agent was evaluated. The tumor images were obtained a few minutes after tail vein injection of 5.0 μmol/kg/B.W of Met-MSN-Gd^{3+}, supporting the utility of Met-MSN-Gd^{3+} as a potential intravascular MRI contrast agent. Clearly, targeting methionine transporters with stable Met-MSN-Gd^{3+} appears to be an efficient route for improving diagnostic cancer in early stage. Finally, the injected dose was lower than the amount of contrast agents that are currently used (0.1–0.3 mmol/kg) [3, 6, 9]. We attributed this to the large pore volume of MSNs for pay-loading of Gd^{3+}-Si-DTPA.

Conclusion

In summary, we have demonstrated that by attaching methionine to the external surface of MSN, one can improve the cellular uptake efficiency of MSN, as well as their ability to escape endosomal compartments. These findings provide helpful insights in the design of efficient contrast agents for nanocarriers delivery.

Acknowledgments. We acknowledge financial support from the Research council of Tehran University of Medical Science. We thank Mr. Behroz Rafiei for his valuable help with the 3T MRI scanner.

Conflict of Interest. All authors declare that they have no conflicts of interest associated with this work.

References

1. Ananta JS, Godin B, Sethi R et al (2010) Geometrical confinement of gadolinium-based contrast agents in nanoporous particles enhances T_1 contrast. Nat Nanotec 5:815–821
2. Taylor KML, Kim JS, Rieter WJ et al (2008) Mesoporous silica nanospheres as highly efficient MRI contrast agents. J Am Chem Soc 130:2154–2155
3. Crich SG, Claudia Cabella C, Barge A et al (2006) In vitro and in vivo magnetic resonance detection of tumor cells by targeting glutamine transporters with Gd-based probes. J Med Chem 49:4926–4936
4. Sun C, Lee JSH, Zhang M (2008) Magnetic nanoparticles in MR imaging and drug delivery. Adv Drug Del Rev 60:1252–1265
5. Slowing II, Trewyn BG, Lin VSY (2008) Mesoporous silica nanoparticles as controlled release drug delivery and gene transfection carriers. Adv Drug Del Rev 60:1278–1288

6. De la Fuente JM, Penad'es S (2006) Glyconanoparticles: Types, synthesis and applications in glycoscience, biomedicine and material science. Biochem Biophys Acta 1760:636–651
7. Shen Z, Li Y, Kohama K et al (2011) Improved drug targeting of cancer cells by utilizing actively targetable folic acid-conjugated albumin nanospheres. Pharmacol Res 63:51–58
8. Eva M, Arto U (2008) Pharmacokinetic role of L-type amino acid transporters LAT1 and LAT2. Eur J Pharm Sci 35:161–174
9. Hyde R, Taylor PM, Hundal HS (2003) Amino acid transporters: roles in amino acid sensing and signaling in animal cells. Biochem J 373:1–18
10. Graf R, Plotkin M, Nyuyki F et al (2012) Contribution of (18)f-fluoro-ethyl-tyrosine positron emission tomography to target volume delineation in stereotactic radiotherapy of malignant cranial base tumours: first clinical experience. Int J Mol Imaging. doi:10.1155/2012/412585
11. Khosroshahi AG, Amanlou M, Sabzevari O et al (2013) A comparative study of two novel nanosized radiolabeled analogues of methionine for SPECT tumor imaging. Cur Med Chem 20:123–133
12. Singhal T, Narayanan TK, Jain V et al (2008) ^{11}C-L-Methionine positron emission tomography in the clinical management of cerebral gliomas. Mol Imaging Biol 10:1–18
13. Dankerl A, Liebisch P, Glatting G et al (2007) Molecular imaging with ^{11}C-methionine PET/CT initial experience. Radiology 242:498–509
14. Schmieder AH, Winter PM, Caruthers SD et al (2005) Molecular MR imaging of melanoma angiogenesis with alphavbeta3-targeted paramagnetic nanoparticles. Magn Reson Med 53:621–627
15. Winter PM, Caruthers SD, Kassner A et al (2003) Molecular imaging of angiogenesis in nascent Vx-2 rabbit tumors using a novel alphavbeta3-targeted nanoparticle. Cancer Res 63:5838–5843
16. Radu DR (2004) Gatekeeping layer effect: a poly (lactic acid)-coated mesoporous silica nanosphere- based flourescence probe for detection of amino-containing neurotransmitters. J Am Chem Soc 126:1640–1641
17. Mehravi B, Ahmadi M, Amanlou M et al (2013) Conjugation of glucosamine on Gd^{3+} based nanoporous silica using heterobifunctional crosslinker (ANB-NOS) for cancer cell imaging. Int J Nanomed 8:3383–3394
18. Erathodiyil N, Ying JY (2011) Functionalization of inorganic nanoparticles for bioimaging. Acc Chem Res 44:925–935
19. Rieter W, Kim JS, Taylor KML et al (2007) Hybrid silica nanoparticles for multimodal imaging. Ange Chem Int Ed 46:3680–3682
20. An Y, Xue MCQ, Liua W (2007) Preparation and self-assembly of carboxylic acid functionalized silica. J Colloid Interface Sci 311:507–513
21. Mehravi B, Ahmadi M, Amanlou M et al (2013) Cellular uptake and imaging studies of glycosylated silica nanoprobe (GSN) in human colon adenocarcinoma (HT 29 Cell line). Int J Nanomed 8:3209–3215
22. Slowing I, Trewyn BG, Lin VSY (2006) Effect of surface functionalization of MCM-41- type mesoporous silica nanoparticles on the endocytosis by human cancer cells. J Am Chem Soc 128:14792–14793
23. Cho Y, Shi R, Borgens RB et al (2008) Functionalized mesoporous silica nanoparticles-based drug delivery system to rescue acrolein-mediated cell death. Nanomed 3(4):507–519
24. Amanlou M, Siadat SD, Ebrahimi SES et al (2011) Gd^{3+} -DTPA-DG: novel nanosized dual anticancer and molecular imaging agent. Int J Nanomed 6:747–763
25. Huang DM, Hung Y, Ko BS et al (2005) Highly efficient cellular labeling of mesoporous nanoparticles in human mesenchymal stem cells: implication for stem cell tracking. FASEB J 19:2014–2016
26. Mirzaei M, Mohagheghi MA, Shahbazi-Gahrouei D (2012) Novel nanosized Gd^{3+}-ALGD-G2-C595: in vivo dual selective MUC-1 positive tumor molecular MR imaging and therapeutic agent. J Nanomed Nanotechol 3:1–6
27. Huang X, Teng X, Chen D et al (2010) The effect of the shape of mesoporous silica nanoparticles on cellular uptake and cell function. Biomaterials 31:438–448
28. Lu J, Liong M, Zink JI, Tamanoi F (2007) Mesoporous silica nanoparticles as a delivery system for hydrophobic anticancer drugs. Small 3:1341–1346